

TRANSITORY CONTROL OF DYNAMIC STALL

George T. K. Woo

George W. Woodruff School of Mechanical Engineering
Georgia Institute of Technology
771 Ferst Drive, Atlanta, Georgia 30332, USA
gtkwoo@gatech.edu

Ari Glezer

George W. Woodruff School of Mechanical Engineering
Georgia Institute of Technology
771 Ferst Drive, Atlanta, Georgia 30332, USA
ari.glezer@me.gatech.edu

ABSTRACT

The flow transients associated with controlled attachment and separation of the flow over a dynamically stalled airfoil are investigated with the objective of enhancing aerodynamic forces and moments. Transitory response to pulsed actuation on time scales that are an order of magnitude shorter than the characteristic convective time scale is assessed. Actuation is effected by time-periodic bursts of momentary [O(1 msec)] pulsed jets that are generated by a spanwise array (0.2 span) of combustion-based actuators integrated into the airfoil. The flow field in the cross stream plane above the airfoil and in its near wake is measured using high-resolution PIV images that are obtained phase-locked to the oscillatory pitch motion of the airfoil, and allow for continuous tracking of vorticity concentrations. The brief actuation pulses lead to remarkably strong changes in the circulation about the entire airfoil that is manifested by manipulation of the surface vorticity layer. It is shown that a burst of a few actuation pulses during the oscillation cycle can lead to a remarkable increase in lift over most of the cycle including at angles of attack that are below stall by trapped vorticity over the entire oscillation cycle.

EXPERIMENTAL SETUP AND PROCEDURES

Controlled, transitory flow attachment for mitigation of dynamic stall are investigated experimentally using a dynamically pitched 2-D NACA-4415 airfoil ($c = 457$ mm, $S = 1$ m). The model is comprised of three spanwise segments where the center segment ($0.21S$, $-0.105S \leq z \leq 0.105S$) is instrumented with a spanwise array of seven combustion-based jet actuators ($x = 0.15c$ from the leading edge, Figure 1). The two outboard segments are unactuated. The experiments are conducted in an open return wind tunnel with a test section measuring 1×1 m and with a free stream velocity, $U_\infty = 20$ m/s ($Re_c = 570,000$ based on the chord length) and the convective time scale of the flow over the airfoil is $T_{conv} = 25$ msec.

The model is mounted on a 2-DOF traverse, which allows for pitch and plunge motions. In the present experiments, the

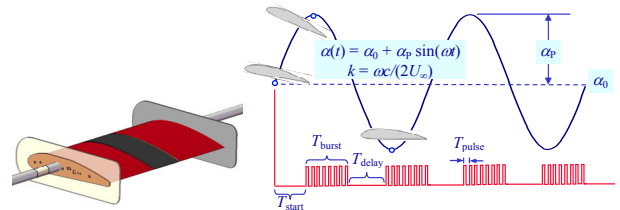


Figure 1. The airfoil assembly and schematic of timing sequence of model motion and actuation.

time-dependent lift $C_L(t)$ and pitching moment $C_M(t)$ are measured independently using load cells and torque sensors that are built into the 2-DOF traverse mechanism. For the dynamic experiments, the model is oscillating about its pitch axis at $\alpha(t) = \alpha_0 + \alpha_p \sin(\omega t)$ where α_0 is the nominal average angle of attack, α_p is the oscillation amplitude, and $k = \omega c / 2U_\infty$ is the reduced frequency. The pitch oscillation range is $10^\circ < \alpha < 18^\circ$, and the cycle period is $T_p = 625$ ms ($T_p = 25T_{conv}$) corresponding to a reduced frequency $k = 0.115$. Figure 1 shows a schematic representation of the oscillatory motion and the general actuation timing used for the control experiments.

The flow over the airfoil and in the wake is characterized using phase-locked particle image velocimetry (PIV) in the cross-stream plane $z = 0$. Measurements across the wake of the airfoil (near its trailing edge) are used to assess the time-dependent circulation about the airfoil.

TRANSITORY CONTROL OF DYNAMIC SEPARATION

As noted above, the present investigation focuses on the flow mechanisms associated with repetitive pulsed actuation and subsequent relaxation of the vorticity layer over a dynamically pitching airfoil beyond its static stall. In particular, the timed interaction between the stall vortex and the actuation are exploited for achieving improved aerodynamic performance and extending flow attachment.

Baseline and Single Pulsed Actuation

Figures 2a-d show C_L (a-b), and $C_{M,c/4}$ (c-d) of the baseline airfoil and in the presence of single-pulse actuation. In the absence of actuation, the lift and pitching moment exhibit hysteretic effects that are associated with dissimilar shedding of vorticity concentrations during the up- and down-strokes of the oscillation cycle (e.g., Woo et al., 2010). Figure 2 also shows the effects of pulsed actuation using a single actuation pulse during the oscillation cycle that is triggered at different delays T_{start} relative to $t = 0$.

In the absence of actuation, the overshoot of C_L above the static level (Figure 2b) is caused by the pitch-up motion of the airfoil beyond the static stall angle ($\alpha \approx 14^\circ$ at $Re_c = 570,000$). Corresponding to the transitory increase in lift, the pitching moment on the airfoil $C_{M,c/4}$ (Figure 2d) remains reasonably invariant. As the airfoil continues to pitch up through $\alpha > 17^\circ$, the lift begins to decrease which is indicative of the onset of stall. Similarly, $C_{M,c/4}$ (Figure 2d) begins to decrease slowly but then exhibits an abrupt drop at $\alpha > 17^\circ$ which is indicative of the onset of moment stall induced by the dynamic shedding of vorticity on the suction surface that is accompanied by an abrupt change in the pressure distribution on the airfoil (Woo et al., 2011). The flow begins to separate once the vortex moves past the trailing edge (at $\alpha < 18^\circ$) until stall is established over a large extent of the suction surface. Flow reattachment begins for $\alpha < 15^\circ$ as lift slowly increases on the latter part of the downstroke. Eventually, the flow returns to unstalled state and the airfoil begins to pitch up and the cycle repeats itself.

The measure of stability in pitch as the angle of attack varies in the presence and absence of actuation can be inferred from the corresponding cyclical changes in the pitching moment. These changes can be related to aerodynamic damping of angular motion about the pitching axis. As described in earlier works (McCroskey, 1982 and Carr, 1988), if the aerodynamic damping is negative during the pitch cycle, these oscillations can amplify and contribute to undesirable dynamic torsion. The control authority of a *single* pulsed jet triggered at different T_{start} is highly dependent on the flow over the airfoil and on the motion of the airfoil. Figure 2 shows the effects of $T_{start} = 0, 30$ and 45, and 60 msec relative to $\alpha_0(t_0) = 14^\circ$ (the cycle-averaged angle of attack). The time traces and phase plots of C_L show that the actuation leads to increased peaks above the baseline, and that these peaks are delayed in accord with the timing of the actuation pulse. In a similar manner, single pulse actuation also affects the pitching moment by significantly reducing the cycle minimum and increasing the cycle maximum levels relative to the baseline. These effects are connected with the transitory interaction between the actuation pulse and the separating shear layer and are augmented by the presence of the dynamic stall vortex. It is conjectured that the flow is beginning to separate on the upstroke for $\alpha \geq \alpha_0$. When the single pulse is applied at short delays ($T_{start} = 0, 30$ and 45ms) relative to t_0 , separation on the suction surface of the airfoil is momentarily suppressed by the actuation, and hence the shedding of the dynamic stall vortex is delayed (at least in the vicinity of the actuator). This

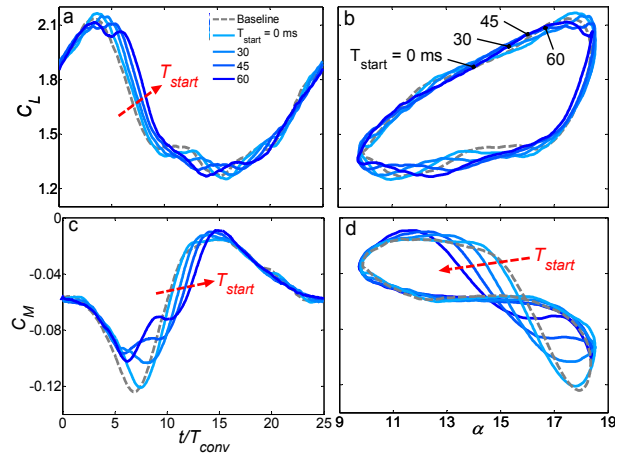


Figure 2. Dynamic lift, C_L (a-b), and moment, $C_{M,c/4}$ (c-d), curves showing the effects of single pulsed actuation applied at several delays $T_{start} = 0, 30, 45, 60$ ms (as marked) relative to the cycle-averaged angle $\alpha_0 = 14^\circ$ and baseline (—).

prolonged trapping of the vortex albeit brief, results in the increase (decrease) in $C_{L,max}$ ($C_{M,c/4,min}$). For $T_{start} = 60$ ms, the small and sharp local peaks in C_L and $C_{M,c/4}$ at $\alpha \approx \alpha_{max}$ in Figures 2b and d suggest that the shedding of the dynamic stall vortex from the leading edge has already begun, but that it is momentarily trapped by the actuation or perhaps even pushed back upstream towards the leading edge. It is important to note that owing to the limited actuation span the single pulsed actuation delays but does not prevent the shedding of the dynamic stall vortex and therefore the onset of stall and full stall flow occur shortly after the termination of actuation. It is noteworthy that the effect of single pulse actuation on shedding of the dynamic stall vortex is further accentuated when the pulse delay relative to α_0 is increased so that the actuation affects the downstroke segment of the pitch cycle (not shown).

Multiple-Pulse Actuation

Motivated by the effective manipulation of the dynamically stalled flow described in the previous section using a single actuation pulse, the effects of repetitive actuation applied in time-periodic bursts relative to the oscillation cycle is investigated. It is noted that repetitive actuation was utilized by Woo et al. (2008 and 2009) to extend significantly the circulation about a stalled static airfoil.

The control authority of a single pulse actuation that covers only a fraction of the stalled flow over the entire airfoil is further exploited by using multiple actuation pulses during the pitch cycle. The first actuation approach is to use N evenly-spaced pulses during the pitch period that are synchronized such that the first pulse is triggered at $t = t_0$. The resulting lift and pitching moment during the pitch cycle are shown in Figure 3 for $N = 5, 10, 15$ and 20 evenly distributed pulses such that the time between successive pulses is $T_{pulse} = 125, 62.5, 41.6,$ and 31.25 msec, respectively. It is evident from the large oscillations in lift and pitching moment for $N = 5$ that the actuation results in large abrupt changes in the flow field above the airfoil. The timing of the actuations is

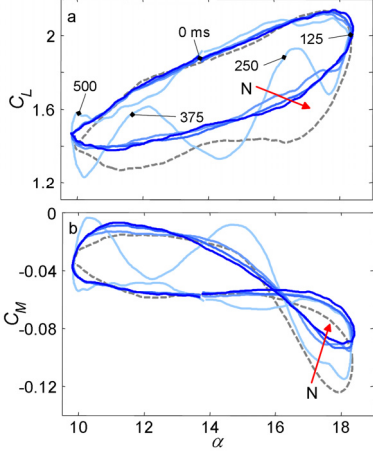


Figure 3. Dynamic lift, C_L , (a) and pitching moment, $C_{M,c/4}$, (b) curves showing the effects of increasing $N=5, 10, 15$ and 20 actuation pulses evenly-distributed around the pitching cycle. The baseline curves are shown (---).

shown in Figure 3a for reference. The effects of the first two pulses following α_0 are similar to the results shown in Figure 2 where the pulsed jets only interact with the flow during the upstroke segment of the cycle. However, the third and fourth pulses are applied during the downstroke segment during the onset of stall. The large changes in C_L and $C_{M,c/4}$ in response to the third pulse indicates the abrupt collapse of the separated flow (at least within the domain that includes the center section of the airfoil) due to the severing of the separating shear layer and the subsequent accumulation of CW vorticity on the airfoil (*cf.* Woo et al., 2008 and 2009 for a static airfoil). The subsequent decrease in C_L and the corresponding increase in pitch up moment are due to the sudden return to stall which is induced by the high pitch angles and the outboard stalled segments of the airfoil (which are not actuated).

It is remarkable that the unsteady effects owing to the 3D interaction with the uncontrolled segments of the airfoil are significantly mitigated when the number of actuation pulses is increased to $N=10$, and as shown in Figure 3, there are no lift and moment oscillations during the pitch cycle. Furthermore, the lift during the entire downstroke half of the cycle is above that of the baseline indicating that dynamic stall is significantly suppressed. At the same time, the undesirable effects of “negative damping” in pitch are significantly reduced. The remarkable improvement in control authority as the number of pulses increases from $N=5$ to 10 is due to the reduction in the elapsed time between successive pulses from $T_{\text{pulse}}/T_{\text{conv}}=5$ to 2.5 (the flow reaches full stall within $4-5 T_{\text{conv}}$ on the downstroke). However, further increases in the number of pulses to $N=15$ or 20 result in relatively small additional increments in C_L and $C_{M,c/4}$ at $\alpha \approx \alpha_{\text{max}}$. In fact, as few as $N=8$ pulses equally distributed through the pitch cycle are sufficient to achieve the bulk of the same increments in C_L and $C_{M,c/4}$. These results indicate that even in the presence of strong 3D effects, tuning the timing of the actuation pulses

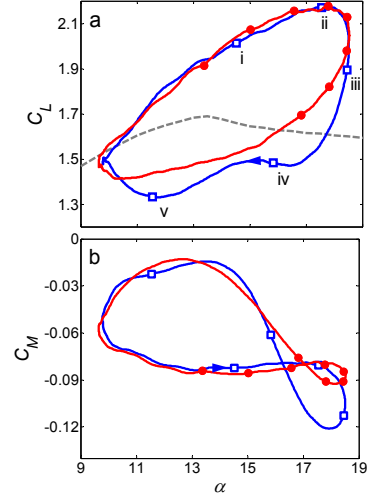


Figure 4. Phase-averaged dynamic lift $C_L(t)$, (a) and pitching moment $C_{M,c/4}(t)$, (b) in the absence (—) and presence of an 8-pulse “staged” actuation sequence (—). The phases of the actuation pulses are marked (●). The corresponding static $C_L(\alpha)$ are shown for reference (---). Five instances during the cycle (i through v) are marked for reference in connection with the discussion of Figures 5, 6 and 7.

during the cycle can lead to an “optimal” pulsed actuation sequence that can effectively control and trap the dynamic stall vorticity concentrations and minimize the actuation power.

Staged Pulse Actuation

The repetitive burst actuation described above, employed pulse sequences that were equally distributed through the pitch cycle. This section considers tuning of the actuation sequence during the pitch cycle. Specifically, the response of the flow to an 8-pulse actuation sequence such that successive pulses are $T_{\text{pulse}}=1.41T_{\text{conv}}$ apart is triggered as the airfoil pitches up through $\alpha=14^\circ$. The actuation is terminated at $\alpha(t=0.36T_p)=16.8^\circ$ during pitch-down. Figure 4 shows that this “staged” 8-pulse sequence not only suppresses the stall oscillation in both the lift and moment, but also reduces the extent of “negative damping” of the pitching moment. The actuation sequence also leads to an increase in lift during the upstroke at high pitch angles. Since the actuation is applied only on the center segment of the airfoil (Figure 1), the data in Figure 4 indicate that even in the presence of strong 3D effects, tuning the timing of the actuation pulses can lead to an “optimal” actuation sequence that can effectively control the flow associated with dynamic stall while minimizing actuation power. In the presence of actuation, the cyclic hysteresis of the dynamic lift ΔC_L decreases by 20% (from 1.02 to 0.82) and the extent of “negative damping” of the pitching moment ΔC_M decreases by 71% (from 0.014 to 0.004). Five instances during the cycle (i through v) are marked for reference in connection with the discussion of Figures 5, 6 and 7.

The effects of the actuation on the flow dynamics over the model during the pitch cycle are captured using PIV

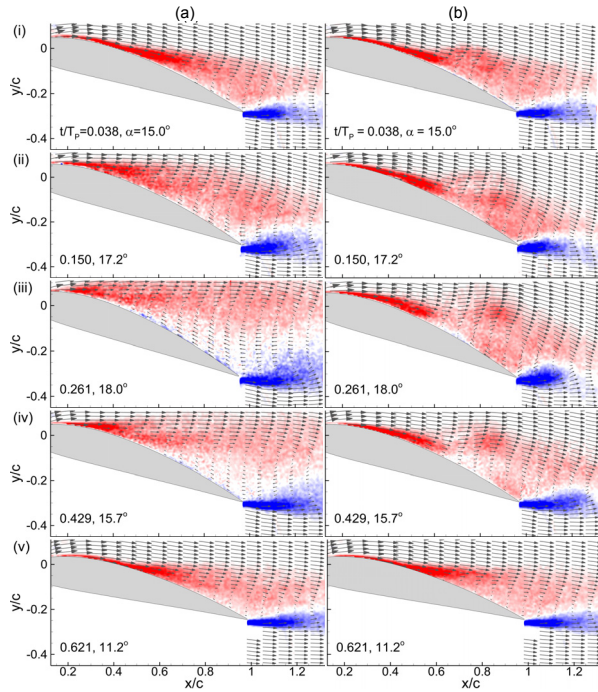


Figure 5. Phase-averaged vorticity maps and velocity distributions above the airfoil and in the near wake during the pitching cycle; baseline (column a) and pulsed actuation (column b). In columns (a) and (b): $\alpha = 15.0^\circ$ ($t/T_p = 0.038$), (i), 17.2° ($t/T_p = 0.150$), (ii), 18° , ($t/T_p = 0.261$), (iii), 15.7° ($t/T_p = 0.429$), (iv) and 11.2° ($t/T_p = 0.621$) (v). Normalized vorticity levels: -40 40

measurements in the cross stream x - y plane at center span ($z = 0$). The measurement domain is $-0.15 < x/c < 1.25$ and $-0.4 < y/c < 0.15$ above the airfoil and in the near wake. The PIV data are acquired phase-locked to the oscillation cycle at 1000 fps with a resolution of $250 \mu\text{m}/\text{pixel}$. The images shown in Figure 5 are color raster plots of the phase-averaged spanwise vorticity concentrations with superposed velocity vectors. The evolution of the flow during five instances of the oscillation cycle that are marked for reference (i through v) in Figure 4 (upstroke: $\alpha = 15, 17.2$ and 18° , and downstroke: $\alpha = 15.7$ and 11.2°) in the absence and presence of actuation are shown in the two columns of Figure 5 [Figures 5a(i - v) and 5b(i - v)], respectively. The images in Figures 5b(i - v) are captured $\Delta t = 0.024T_p$ following the 1st, 3rd, 5th, and 8th actuation pulses while the images in Figures 5a-v and b-v are captured at $t = 0.621T_p$ when the airfoil pitches down through 11.2° for the two flows.

In the absence of actuation, the flow at $\alpha(t/T_p = 0.038) = 15^\circ$ (Figure 5a-i) appears to be attached over most of the suction surface although the boundary layer thickens considerably towards the trailing edge while the corresponding flow over the static airfoil is stalled (*cf.* Figure 4a). As the airfoil continues to pitch up through $\alpha(t/T_p = 0.150) = 17.2^\circ$ (Figure 5a-ii), a recirculating flow domain appears at $x/c > 0.6$ and extends beyond the trailing edge of the airfoil. The baseline flow (at center span) is fully

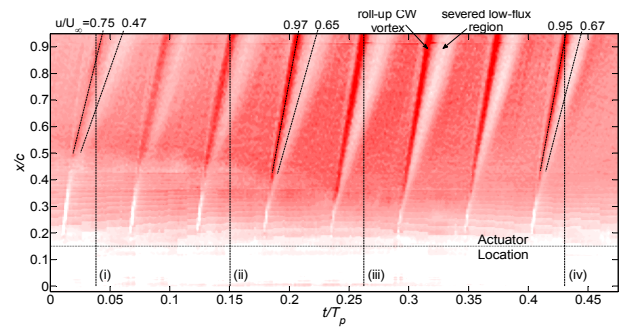


Figure 6. x - t raster plots of phase-averaged vorticity flux for 8-pulse actuation showing propagation velocities of the induced CW vorticity concentrations. Normalized vorticity flux levels: -1.5 0.5

separated at $\alpha(t/T_p = 0.261) = 18^\circ$ (Figure 5a-iii). Although the separation over the baseline airfoil is three-dimensional and appears first near center span (Woo et al., 2011), the measured C_L in Figure 4a indicates a characteristic feature of dynamic stall in that concentrations of CW vorticity accumulated during pitch up cycle are still present and the loss in lift is minimal. At $t/T_p = 0.429$, as the airfoil pitches down through $\alpha = 15.7^\circ$, the flow above the airfoil remains separated (Figure 5a-iv) although the separating shear layer and the flow above it appear to be deflected towards the airfoil. However, the massive shedding of vorticity following the onset of stall results in a significant reduction in C_L and in ‘negative damping’ in pitch (Figure 4b). Finally at $t/T_p = 0.621$ (pitch down through $\alpha = 11.2^\circ$), the flow re-attaches over the entire surface of the airfoil (Figure 5a-v) although C_L is lower than during the upstroke (Figure 4a).

The response of the flow to the actuation sequence (*cf.* Figure 4) is shown in Figures 5b-i through 5b-v. Figure 5b-i ($\alpha = 15^\circ$) shows the response to the first actuation pulse and the rollup and advection of a CW vortex that is embedded within the surface vorticity layer as the airfoil continues to pitch up. This image indicates that the boundary layer upstream of the CW vortex is somewhat thinner than in the absence of actuation (Figure 5a-i). It is remarkable that the advection speed of the vortex is such that its interaction with the upstream boundary layer promotes flow attachment indicating that the interaction results in a favorable pressure gradient. The advection of the CW vortex that is formed following the third actuation pulse is shown in Figure 5b-ii ($\alpha = 17.2^\circ$). Again, in comparison to the baseline flow (Figure 5a-ii) which is close to stall, the boundary layer upstream of the CW vortex in Figure 5b-ii is much thinner. Of particular note is the trapped CW vorticity concentration upstream of the trailing edge after the shedding of the actuation-induced vortex which is similar to, though smaller in extent than the trailing edge vortex in the baseline flow that is associated with dynamic stall. Furthermore, the controlled shedding of CW vorticity apparently suppresses the abrupt changes in the pressure distribution on the suction surface and hence significantly reduces the extent of ‘negative damping’ in Figure 4b. A similar pattern continues following the fifth

actuation pulse in Figure 5b-iii ($\alpha = 18^\circ$) which highlight the significant suppression of separation in comparison to the baseline flow (Figure 5a-iii). Note that the actuation-induced CW vortex is significantly larger than at lower angles of attack. The evolution of the flow following the eighth (and last) actuation pulse is shown in Figure 5b-iv ($\alpha = 15.7^\circ$). While the extent of the separation in the baseline flow is beginning to diminish as the downstroke progresses, the actuation still results in transitory, progressive flow attachment (Figure 5b-iv). Finally, at $t/T_p = 0.621$ (pitch down through $\alpha = 11.2^\circ$), following the termination of the actuation, the actuated flow [Figure 5b-v ($\alpha = 11.2^\circ$)] is reattached over the entire surface of the airfoil and is very similar to the baseline flow (Figure 5a-v). However, it is noteworthy that the C_L in the presence of actuation is higher than at the corresponding downstroke angle in the baseline flow (Figure 4a). This indicates that in the presence of actuation the cycle-averaged trapped vorticity is higher than for the baseline flow.

It is instructive to assess the evolution of the vorticity layer above the airfoil using an $x-t$ diagram of the vorticity flux through vertical cross-stream sections of the measurement domain ($0 < x/c < 1.2$) as shown in Figure 6. The phase points during the airfoil's oscillation cycle that are marked in Figure 4 are shown by dashed lines. The important features are the changes in the advection speeds following successive actuation pulses. Figure 6 shows that for the first pulse, the CW vortex remains close to the suction surface and has a characteristic propagation velocity $u_{adv}/U_\infty \approx 0.75$ [cf. $u_{adv}/U_\infty \approx 0.75$ for a single pulse over a static airfoil (Woo et al., 2009)]. These data shows that the CW vortex induced by the 4th actuation pulse is advected at a higher speed ($u_{adv}/U_\infty \approx 0.97$) due to its closer proximity to the free stream flow while the flow over the airfoil appears to be separated. As expected, the vortex induced by the last (8th) pulse is advected at a lower speed ($u_{adv}/U_\infty \approx 0.95$) due to the pitch-down motion of the airfoil. Perhaps the most prominent feature in the $x-t$ diagram, is the appearance of streaks of low vorticity flux that is associated with the severing and rollup of the separated CW vorticity layer. The characteristic speeds of the streaks following the 1st, 4th and 8th actuation pulses are $u_{adv}/U_\infty = 0.47, 0.65$ and 0.67 , respectively. It is owing to the differences in the characteristic propagation velocities that the severed region is stretched in the streamwise direction as indicated in Figure 6 by the increase in its width with t/T_p . This streamwise stretching represents the growth of the upstream boundary layer following each pulse, and the disparity between the amount of CW vorticity shed by the vortices and the accumulation of CW vorticity on the suction surface. This $x-t$ diagram indicates that there are no pairings or amalgamations of the CW vortices within the measurement domain (cf. Woo et al., 2009). It shows that as the actuation sequence progresses, the flux intensifies momentarily, and then subsides indicating temporal accumulation of vorticity that is also evident in Figure 7.

The global aerodynamic performance of the moving airfoil is quantified by considering the time-evolution of the phase-averaged cross-stream distributions of the vorticity flux $\omega_z u$

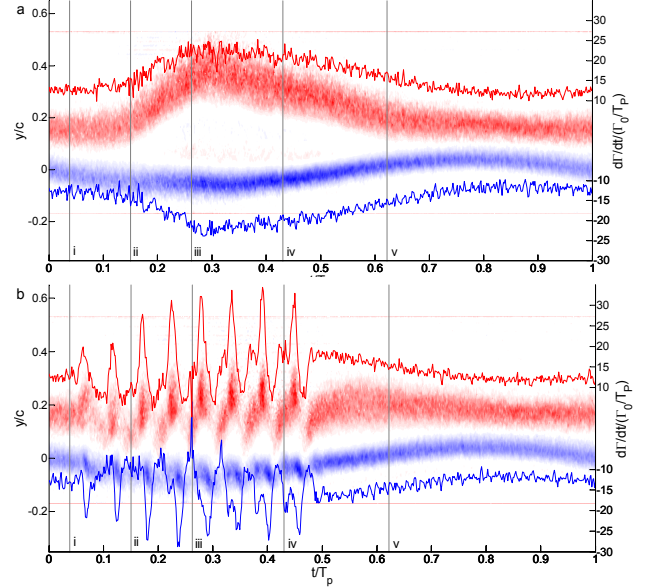


Figure 7. Raster plots of the phase-averaged cross-stream distribution of vorticity flux (CW and CCW) during the pitching cycle measured at $x/c = 0.25$ downstream of the trailing edge in the absence (a) and presence (b) of actuation. Included are the corresponding line traces of the time-rate change of circulation, $(d\Gamma/dt)_{CW}$ and $(d\Gamma/dt)_{CCW}$. Reference five instances from Figure 4.(i - v) are also marked.

(CW and CCW from the suction and pressure surfaces) downstream of the trailing edge (at $x/c = 1.25$) as shown in Figures 7a and b. Time instances i through v in Figures 4, 5 and 6 are also marked for reference. In the absence of actuation (Figure 7a), the changes in the cross stream width of the wake for $t < 0.18 T_p$ are relatively small indicating a reasonably attached flow during this part of the upstroke. However, when the flow begins to separate the cross-stream extent of the wake increases rapidly along with the magnitude of the flux of CW vorticity which is associated with the shedding of the vorticity concentration from dynamic stall (at about $t/T_p = 0.18$ $\alpha \approx 17^\circ$ during the downstroke, cf., Figure 4). The maximum broadening of the wake occurs at $0.36 \leq t \leq 0.38 T_p$ corresponding to full stall. Thereafter, the flow slowly reattaches as the airfoil continues to pitch down.

The corresponding cross stream distributions of the vorticity flux in the presence of actuation (Figure 7b) exhibit two striking differences compared to the baseline flow. First, the sequence of eight actuation pulses clearly modulates the vorticity fluxes from *both* the suction and pressure surfaces of the airfoil. Second, and perhaps more striking, is the absence of massive stall as indicated by the widening of the wake. The time rate of change of the airfoil's circulation for the baseline and actuated flows is computed by integration of vorticity flux across the wake $d\Gamma/dt = -\int(\omega_z u) dy$, and traces of normalized $(d\Gamma/dt)_{CW}$ and $(d\Gamma/dt)_{CCW}$ are also shown in Figures 7a and b. It is interesting to note that in the absence of actuation, the magnitudes of $(d\Gamma/dt)_{CW}$ and $(d\Gamma/dt)_{CCW}$ are similar and that the vorticity flux from the suction side intensifies during the

downstroke. It is evident that the sum ($d\Gamma/dt$) is associated with a net increase in circulation as shown in Figure 8. As noted above, the vorticity flux into the wake is altered significantly in the presence of actuation. The time rate of change of the circulation that is associated with the shedding of the discrete vortices induced by the actuation pulses increases as the actuation progresses and appears to reach a maximum level when the airfoil attains its largest angle of attack before the beginning of the downstroke. It is remarkable that the strength of the shed CW vortices (which is clearly coupled to the motion of the airfoil) is nearly invariant during the downstroke.

Finally, the time-dependent circulation increment that is computed relative to the circulation when the airfoil pitches up through $\alpha = \alpha_o$, $-\Delta\Gamma(t)$ is shown in Figure 8a in the absence and presence of actuation. The initial rise in circulation ($0 \leq t \leq 0.16T_p$) for the baseline (unactuated) motion corresponds to the accumulation of CW vorticity during the formation of the dynamic stall vortex ($-\Delta\Gamma_{\max}/\Gamma_o \approx 0.09$ at $t \approx 0.12T_p$). The subsequent reduction in circulation ($0.16 \leq t \leq 0.56T_p$) is due to the shedding of accumulated dynamic stall vorticity and the onset of stall over the airfoil at $t \approx 0.56T_p$ before the flow reattaches again ($-\Delta\Gamma$ vanishes) as the pitching cycle continues. In the presence of actuation, the circulation exhibits oscillations that are induced by the actuation pulses as the circulation level increases relative to $\alpha = \alpha_o$, $t = 0$, but the increase is significantly larger compared to the baseline ($-\Delta\Gamma_{\max}/\Gamma_o \approx 0.25$ at $t \approx 0.3T_p$) and lasts for the duration of the actuation through $t \approx 0.52T_p$. Following the termination of the actuation as the airfoil continues to pitch, there is a reduction in circulation ($-\Delta\Gamma_{\min}/\Gamma_o \approx -0.13$ at $t \approx 0.64T_p$), but this reduction is significantly smaller than the corresponding reduction of the baseline pitch indicating that the effects of the actuation lasts beyond its termination and consequently a cycle-averaged increase in circulation owing to the actuation. In addition, the control authority of the actuation is evident in Figure 8b that shows the phase-averaged net change in global circulation relative to the baseline during the pitching cycle. Even though the circulation is only computed at center span and the effect of the actuation clearly varies across the span owing to three-dimensional effects, it is remarkable that an eight-pulse sequence that is applied during the upstroke and lasts for about 40% of the cycle period leads to an increase in circulation through almost the entire cycle. The net circulation build-up during actuation is rapid, reaching a maximum level (at $t \approx 0.3T_p$) which is equivalent to an increase of 33% when normalized by $\Gamma_o(t_o)$, before decreasing upon termination of actuation and the end of the pitch cycle.

CONCLUSIONS

Transient aerodynamic control of the flow over a 2-D airfoil undergoing oscillatory ($k = 0.115$) pitch is investigated in wind tunnel experiments using pulsed actuation. The actuation is effected over the center segment of the airfoil's span ($0.21S$) by a spanwise array of, combustion-based jets having a characteristic time scale that is an order of magnitude

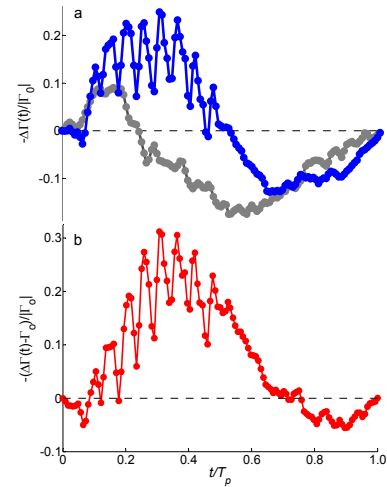


Figure 8. a) Phase-averaged circulation increment for the baseline cycle in the absence of actuation (\bullet) and with pulsed actuation (\bullet), and b) Phase-averaged net change in global circulation due to the actuation relative to the baseline (\bullet).

shorter than the convective time scale of the flow. It is shown that the aerodynamic performance is significantly enhanced in response to a burst of eight repetitive actuation pulses $1.41T_{\text{conv}}$ apart. The actuation mitigates hysteretic effects that are associated with dissimilar shedding of vorticity concentrations during the up- and down-strokes of the oscillation cycle of the baseline airfoil. As a result, the cyclic lift is increased by 20% and the extent of “negative damping” of the pitching moment is decreased by 71% relative to the baseline. Detailed, phase-locked PIV measurements of the flow field over the airfoil at center-span and in its near wake show that the dynamically separated flow is controlled by effective trapping of vorticity concentrations over the airfoil as a result of the successive actuation. Finally, it is also shown that compared to the baseline flow, in the presence of the actuation the circulation (measured in the center cross stream plane $z = 0$) increases during most of the pitching cycle by as much as 33%.

REFERENCES

- Carr, L. W., “Progress in Analysis and Prediction of Dynamic Stall,” *Journal of Aircraft*, **25-No.1**, 6-17, 1988.
- McCroskey, W. J., “Unsteady Airfoils,” *Ann. Rev. of Fluid Mechanics*, **14**, 285-311, 1982.
- Woo, G. T. K., Crittenden, T., and Glezer, A., “Transitory Control of a Pitching Airfoil using Pulse Combustion Actuation,” AIAA Paper 08-4324, 2008.
- Woo, G. T. K., Crittenden, T., and Glezer, A., “Transitory Separation Control over a Stalled Airfoil,” AIAA Paper 09-4281, 2009.
- Woo, G. T. K., and Glezer, A., “Transient Control of Separating Flow over a Dynamically-Pitching Airfoil,” AIAA Paper 2010-861, 2010.
- Woo, G. T. K., Crittenden, T., and Glezer, A., “Transitory Control of Dynamic Stall on a Moving Airfoil,” AIAA Paper 2011-0489, 2011.